

Unpacking drivers of heterotrophic N₂ fixation across aquatic redox gradients: A mathematical model with bioenergetic and stoichiometric constraints

Corday R. Selden^{a, #, *}, Rebecca A. Everett^{b, #, *}, Halvor M. Halvorson^c, Megan E. Berberich^d, Luca Schenone^{e, f}, Angela Peace^g, Renn Schipper^h, Edwin Cruz-Riveraⁱ, James Powell^j, Keisuke Inomura^k, Robinson W. Fulweiler^{l, n}, Amy M. Marcarelli^d, J. Thad Scott^m

^a Department of Marine and Coastal Sciences, Rutgers University, New Brunswick, NJ, United States

^b Department of Mathematics and Statistics, Haverford College, Haverford, PA, United States

^c Department of Biology, University of Central Arkansas, Conway, AR, United States

^d Department of Biological Sciences, Michigan Technological University, Houghton, MI, United States

^e Laboratorio de Limnología, INIBIOMA-CONICET, Universidad Nacional del Comahue, Bariloche, Argentina

^f Limnological Institute, University of Konstanz, Konstanz, Germany

^g Department of Mathematics and Statistics, Texas Tech University, Lubbock, TX, United States

^h Department of Biological Sciences, Kent State University, Kent, OH, United States

ⁱ Department of Biology, Morgan State University, Baltimore, MD, United States

^j Center for Marine and Environmental Studies, University of the Virgin Islands, St. Thomas, VI, United States

^k Graduate School of Oceanography, University of Rhode Island, Narragansett, RI, United States

^l Department of Earth and Environment, Boston University, Boston, MA, United States

^m Department of Biology, Baylor University, Waco, TX, United States

ⁿ Department of Earth and Environment, Department of Biology, Boston University, Boston, MA, United States

ARTICLE INFO

Keywords:

Diazotroph
Organic matter
Nitrogen cycle
Sediments
Energetics
Gradients
Azotobacter
Droop model
Ecological stoichiometry

ABSTRACT

N₂ fixation by aquatic organoheterotrophs supplies bioavailable nitrogen to the biosphere and thereby supports ecosystem production; yet the factors which drive this activity are poorly understood. Here, we present a generalized chemostat model to investigate stoichiometric and energetic constraints on free-living heterotrophic diazotrophs across gradients in redox state, resource quantity/quality, and resource stoichiometry. The model couples nutrient uptake and allocation functions to predict elemental fluxes with an energy dissipation model to calculate growth efficiency. After constraining model parameters with relevant culturing (e.g., *Azotobacter*) and environmental literature, we assessed model sensitivity to these parameters using Latin Hypercube Sampling and the statistical Partial Rank Correlation Coefficient technique. Consistent with the limited observational data available, the results showed energy acquisition and respiratory efficiency as two major controls on N₂ fixation. The model predicted the presence of N₂ fixation under both N-limiting and N-replete conditions, as seen in nature. N₂ fixation under N-replete conditions increased with increasing resource C:N, and was least sensitive to exogenous N under eutrophic conditions with an energy-rich C source. While N₂ fixation under N-replete conditions represented a relatively small (<4 %) contribution to community N demand, absolute rates under these conditions were on par with field observations under N-limitation due to higher overall heterotrophic production rates. Resolving physiological, stoichiometric, and energetic constraints on diazotrophic growth, this model unpacks drivers of N₂ fixation by metabolically diverse heterotrophs.

* Corresponding authors.

E-mail addresses: crselden@marine.rutgers.edu (C.R. Selden), reverett@haverford.edu (R.A. Everett).

These authors contributed equally.

<https://doi.org/10.1016/j.ecolmodel.2025.111454>

Received 20 June 2025; Received in revised form 4 December 2025; Accepted 9 December 2025

Available online 19 December 2025

0304-3800/© 2025 The Authors. Published by Elsevier B.V. This is an open access article under the CC BY license (<http://creativecommons.org/licenses/by/4.0/>).

1. Introduction

Diazotrophs are prokaryotes capable of converting dinitrogen (N_2) gas to ammonium, supplying bioavailable nitrogen (N) and thus supporting ecosystem production (Marcarelli et al., 2022). This functionally diverse group (Inomura et al., 2020) varies greatly in their niche preferences and ecophysiology (Koirala and Brözel, 2021). In both the aquatic and terrestrial biosphere, many diazotrophs consume organic matter to acquire energy and elements required for growth and N_2 fixation (organoheterotrophic diazotrophs, hereafter ‘heterotrophs’) (Pierella Karlusich et al., 2021). These organisms have long been known to contribute significantly to the terrestrial N budget (Vitousek et al., 2013). In the ocean too, presumably heterotrophic non-cyanobacterial diazotrophs are now known to be widespread (Turk-Kubo et al., 2022) and recent modeling work indicates that heterotrophs contribute ~10% of marine N_2 fixation globally (Chakraborty et al., 2025). Yet, despite their probable importance, the contribution and environmental drivers of heterotrophic N_2 fixation in historically under-sampled but impactful (Fulweiler et al., 2025) inland and coastal waters remains poorly constrained.

Inland and coastal waters (including the sediments and waters of rivers, wetlands, estuaries, and continental shelf environments) span pronounced gradients in redox state, nutrient availability, and organic matter richness/quality which shape microbial habitat and biogeochemical activity. In contrast to the long-held belief that fixed N precludes N_2 fixation, both observations (e.g., Bentzon-Tilia et al., 2015a; Fulweiler et al., 2013; Selden et al., 2019, 2021) and models (e.g., Chakraborty et al., 2021; Inomura et al., 2018) hint that heterotrophic N_2 fixation can occur in the presence of fixed N, particularly where oxygen (O_2) concentrations are low to nil and organic matter is bountiful (Fulweiler, 2023). Across aquatic environments, the form and lability of organic compounds for respiration can vary significantly, driving variability in heterotroph growth efficiency and production through time and space (Del Giorgio and Davis, 2003; Del Giorgio and Cole, 1998). This study sought to unpack how mechanistic controls on N_2 fixation vary across chemical gradients in heterogeneous sediments and waters along the aquatic continuum—environments where data is sparse and from which few heterotrophic diazotrophs have been investigated in culture.

Gibbs energy dissipation models (GEDMs) (Heijnen et al., 1992; Heijnen and Van Dijken, 1992) offer a “first principles” framework to represent microbial bioenergetics in diverse chemical environments. Founded in thermodynamic theory, GEDMs derive maximum bacterial growth yield (i.e., growth efficiency) from the free energy produced during the breakdown of carbon (C) substrates (catabolism) and the free energy consumed in biomass construction and maintenance reactions (anabolism). GEDMs have been successfully applied to investigate growth dynamics of a myriad of low energy-yield metabolisms, including denitrification (González-Cabaleiro et al., 2015) and sulfate reduction (Smeaton and Van Cappellen, 2018).

Yet, bioenergetics is not the only constraint—environmental stoichiometry has long been viewed as the major driver of new N inputs via N_2 fixation (e.g., Redfield, 1958). A limitation of the GEDM approach is that it fails to consider the relative availability of substrates for growth, as well as kinetic constraints on substrate uptake. Stoichiometric models (Hessen et al., 2013; Sterner and Elser, 2003), conversely, use a mass balance approach to assess how elemental imbalances affect biological processes across hierarchical scales of organization, yet they traditionally apply no bioenergetic constraints.

Building upon GEDMs framework by incorporating varied stoichiometry, here we present a generalized chemostat-type model of heterotrophic N_2 fixation. The model combines (1) a GEDM approach to calculate growth yields from thermodynamic theory and (2) an empirical mathematical model with kinetic and variable stoichiometric constraints to predict elemental fluxes. This approach predicts dynamics of free-living heterotrophic diazotroph populations capable of respiring

dissolved oxygen (O_2), nitrate (NO_3^-), or sulfate (SO_4^{2-}) across redox gradients in aquatic environments. We perform sensitivity analysis to pin down impactful trait parameters on N_2 fixation and N:C (carbon) ratios of heterotrophic diazotrophs under five representative habitats.

2. Materials and methods

2.1. Model overview

The model (Fig. 1) describes the growth and biogeochemical activity of a population of heterotrophs, composed of both aerobes and anaerobes, as a function of the availability and speciation of substrates for catabolism (energy production) and anabolism (biomass construction). We consider three environmental N (Ne) sources—nitrate (Ne_{NO_3}), ammonium (Ne_{NH_4}), and N_2 gas (Ne_{N_2})—which are tracked into N biomass (Nb ; as Nb_{NO_3} , Nb_{NH_4} , and Nb_{N_2} , respectively). Three respiratory pathways are represented using the terminal electron acceptors (TEAs) O_2 , NO_3^- , and SO_4^{2-} . Of these substrates, only N_2 and SO_4^{2-} are considered as non-exhaustible pools as these are typically abundant in aquatic systems; however, we note that SO_4^{2-} concentrations can be drawn down in some freshwaters and caution must thus be taken if applying the model in any such system. Theoretical growth yield is determined instantaneously as a function of anabolic energy consumption and dissipative energy loss relative to the potential energy gain of catabolism (see Section 2.2); realized growth yield includes additional respiratory costs associated with N_2 fixation (see Eqns. (2) and 12) and, along with substrate availability and $Q_{Nb,Cb}$, controls population growth rate (Eqn. (6)). Thermodynamic values to calculate theoretical growth yields assumed standard conditions (25 °C).

Our aim in this study was to model a generalized population of heterotrophic diazotrophs to investigate key drivers of their activity across redox gradients. To cope with the dearth of data available on heterotrophic diazotroph physiology, which is likely quite variable (Bentzon-Tilia et al., 2015a; Castillo et al., 2020), growth energetics are constrained using a “first principles” approach which is not organism- or ecosystem-specific (Section 2.2). Substrate uptake kinetics are derived using Michaelis-Menten-type equations (see Sections 2.3–2.5) (Michaelis and Menten, 1913) while Droop-type equations (Droop, 1973) constrain substrate uptake as a function of the internal nutrient pool, specifically the molar N:C ratio of biomass ($Q_{Nb,Cb}$). Given the sparsity of data available to parameterize the stoichiometric model, we systematically collated a range of values from appropriate literature (Section 2.6) and then assessed the sensitivity of the model to each parameter using these ranges (Section 2.7) under varied environmental scenarios (detailed in Section 2.8). To collate a range of appropriate values for each parameter, we first sought to leverage the long history of physiological research on the model heterotrophic diazotroph *Azotobacter vinelandii*, and then expanded our search by looking for data on aquatic heterotrophs more generally (see Section 2.6 and Supplemental D for details and limitations).

The full list of model equations is given in Supplemental A. Section 2.9 discusses model limitations.

2.2. Calculating bacterial growth yields from first principles

Gibbs free energy (G) is defined as the energy available in a chemical system to do work. When a reaction proceeds, the difference in the Gibbs free energy between the products and reactants (ΔG) reflects the energy liberated ($-\Delta G$) or consumed ($+\Delta G$) by the reaction, and indicates whether the reaction can proceed spontaneously i.e., without exogenous energy input. To grow, microorganisms must harvest sufficient energy through catabolic reactions (ΔG_{cat} ; units = kJ/C-mol electron donor) to support cell maintenance and drive growth via anabolic reactions (ΔG_{ana} ; units = kJ/C-mol biomass). Additionally, some portion of the energy harvested through catabolism is lost due to dissipative processes (ΔG_{dis} ; units = kJ/C-mol biomass).

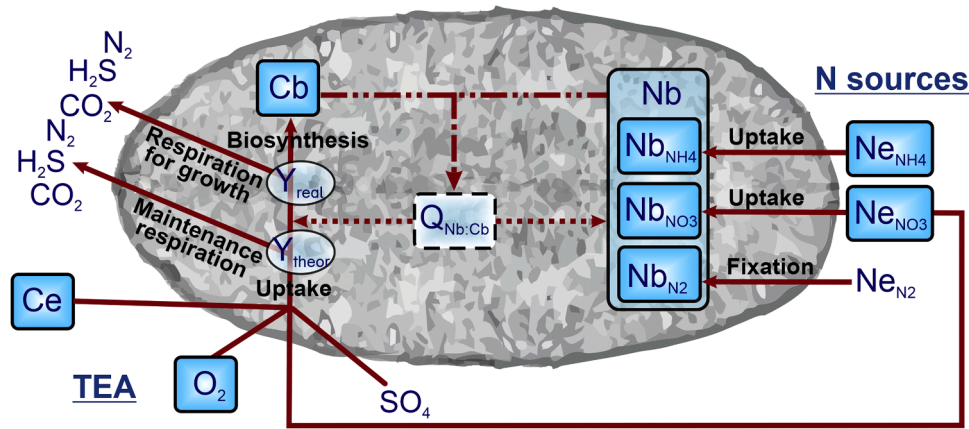


Fig. 1. Conceptual model of N_2 fixation in mixed population of heterotrophic facultative anaerobes under chemostat. Closed light-blue boxes represent dynamic compartments: environmental ammonium (Ne_{NH_4}), environmental nitrate (Ne_{NO_3}), atmospheric oxygen (O_2), environmental organic carbon (Ce), and carbon in biomass (Cb); nitrogen in biomass (Nb) includes N derived from ammonium uptake (Nb_{NH_4}), nitrate uptake (Nb_{NO_3}) and N_2 fixation (Nb_{N_2}). Solid arrows represent mass flux and dashed arrows represent the stoichiometric control, where the biomass nitrogen to carbon ratio is given by $Q_{Nb,Cb}$. The terminal electron acceptors (TEA) are O_2 , Ne_{NO_3} , and environmental sulfate (SO_4). Y_{theor} and Y_{real} represent the theoretical and realized growth yields, respectively.

To assess how variability in catabolic and anabolic pathways affect the growth, biogeochemical activity, and stoichiometry of heterotrophic diazotrophs across high- to low-energy yield environments, we calculated theoretical growth yields (Y_{theor}) in units of C-mol biomass/C-mol electron donor as follows:

$$Y_{theor} = \frac{\Delta G_{cat}}{-\Delta G_{dis} + \Delta G_{cat} * V - \Delta G_{ana}} * \frac{1}{n} \quad (1)$$

where n represents the number of C atoms in the C source ($n=2$ for acetate and 6 for glucose) and V (Table 1) is a stoichiometric coefficient indicating the molar amount of electron donor required to synthesize 1 C-mol biomass derived from the anabolic reaction (Heijnen et al., 1992). This value represents the theoretical upper limit for bacterial growth efficiency. ΔG values (Table 1) were derived as described in Suppl. Text B1. As described in Section 2.3, we use Y_{theor} to derive a realized yield (Y_{real}), which accounts for additional costs of cellular maintenance processes, including the additional respiratory burden of protecting nitrogenase from oxidative damage under high O_2 conditions (Poole and Hill, 1997; Sabra et al., 2000). This value directly couples the rate of substrate consumption to biomass growth rate, and is used to calculate realized growth rates ($\frac{dCb}{dt}$).

2.3. Equations for realized growth and carbon uptake

True bacterial growth yield includes not only the relevant energetics of catabolism and anabolism, but also the additional costs of cellular maintenance processes i.e., basal metabolism. Realized yield (Y_{real} ; units are C-mol biomass/C-mol electron donor) was consequently calculated from Y_{theor} as follows:

$$Y_{real} = Y_{theor} * \frac{[C \text{ uptake rate}_{non-basal}]}{[C \text{ uptake rate}_{total}]}, \quad (2)$$

where total C uptake rate accounts for three fates of C: (a) respiration to meet the energy demand of growth, (b) respiration for basal metabolism and respiratory protection, and (c) anabolic C assimilation. The numerator in Eqn. (2) represents fates (a) and (c) (see Eqn. (3)); the denominator represents the sum of all three pathways (see Eqn. (4)).

Here, we consider C uptake rate to be a function of TEA availability in the environment, C substrate availability in the environment, and the C demand of the population, which itself depends upon the N:C ratio of biomass ($Q_{Nb,Cb}$). We define the rate of C uptake (in units of mol C L⁻¹ d⁻¹) for non-basal metabolism as:

Table 1
Catabolic and anabolic reactions included in the model with associated Gibbs free energies.

Reaction type	Carbon source	Electron acceptor (catabolic) or N source (anabolic)	Equation	V (moles electron donor per C-mol biomass)	ΔG°	Unit
Catabolic	Acetate ($C_2H_3O_2^{-1}$)	O_2	$C_2H_3O_2 + 2O_2 \rightarrow 2HCO_3 + H^+$	-	-844.3	kJ mol ED ⁻¹
		NO_3^-	$C_2H_3O_2 + 1.6NO_3 + 0.6H^+ \rightarrow 2HCO_3 + 0.8N_2 + H_2O$	-	-792.14	
	SO_4^{2-}	$C_2H_3O_2 + SO_4^{2-} \rightarrow 2HCO_3 + HS^-$	-	-47.7		
	O_2	$C_6H_{12}O_6 + 6O_2 \rightarrow 6HCO_3 + 6H^+$	-	-2841.0		
	NO_3^-	$C_6H_{12}O_6 + 4.8NO_3 \rightarrow 6HCO_3 + 2.4N_2 + 2.4H_2O + 1.2H^+$	-	-2684.5		
Anabolic	Acetate ($C_2H_3O_2^{-1}$)	NH_4^+	$0.525C_2H_3O_2 + 0.2NH_4^+ + 0.275H^+ \rightarrow$	0.525	29.6	kJ C-mol biomass ⁻¹
		NO_3^-	$CH_{1.8}O_{0.5}N_{0.2} + 0.05HCO_3 + 4H_2O$	-	87.6	
	N_2		-	110.4		
	NH_4^+	$0.175C_6H_{12}O_6 + 0.2NH_4^+ \rightarrow$	0.175	-24.4		
	NO_3^-	$CH_{1.8}O_{0.5}N_{0.2} + 0.05HCO_3 + 0.25H^+ +$	-	33.3		
Dissipation	Acetate ($C_2H_3O_2^{-1}$)	-	-	-	529	kJ C-mol biomass ⁻¹
		-	-	-	284	
	Glucose ($C_6H_{12}O_6$)	-	-	-	284	

$$C \text{ uptake rate}_{\text{non-basal}} = \left[(r_{O_2} + r_{NO_3} + r_{SO_4}) * \left(\frac{Ce}{K_r + Ce} \right) * \left(1 - \frac{Q_{min}}{Q_{Nb,Cb}} \right) * Cb \right] \quad (3)$$

and total C uptake rate (mol C L⁻¹ d⁻¹) is expressed as:

$$C \text{ uptake rate}_{\text{total}} = \left[(r_{O_2} + r_{NO_3} + r_{SO_4}) * \left(\frac{Ce}{K_r + Ce} \right) * \left(1 - \frac{Q_{min}}{Q_{Nb,Cb}} \right) * Cb \right] + \left[(m_{O_2} + m_{NO_3} + m_{SO_4}) * \left(\frac{Ce}{K_m + Ce} \right) * Cb \right], \quad (4)$$

where Ce and Cb indicate the molar quantity of C in the environmental substrate pool (glucose, acetate) and biomass, respectively, K_r is the half-saturation constant for C uptake, and Q_{min} is the minimum allowable N:C ratio of biomass. The terms $(r_{O_2} + r_{NO_3} + r_{SO_4})$ and $(m_{O_2} + m_{NO_3} + m_{SO_4})$ describe the amount of respiration to fuel growth/biosynthesis (i.e., non-basal metabolism) and maintenance processes (i.e., basal metabolism) that is accounted for by each TEA (in C-mol equivalents). These rates are separated as the availability of each oxidant may limit C uptake via its particular respiratory pathway, and because the community transitions smoothly from one TEA to the next. See Section 2.4 for further details on respiration.

Taking a chemostat-type arrangement which accounts for cell death (δ) and dilution (D), the concentration of C substrate in the environment (Ce) increases by inflow and regeneration of biomass C, and decreases by outflow and biological C uptake:

$$\frac{dCe}{dt} = D * Ce_{in} + \delta * Cb - [C \text{ uptake rate}_{\text{total}}] - D * Ce, \quad (5)$$

where Ce is the instantaneous C concentration in the environment and Ce_{in} is the “media” molar concentration i.e., the resupply concentration. Regeneration is assumed to be instantaneous and produces the same carbon substrate as in the influx medium. Finally, growth rate, presented here as a change in biomass C (Cb) per time ($\frac{dCb}{dt}$; units are mol C L⁻¹ d⁻¹), can be calculated as:

$$\frac{dCb}{dt} = Y_{real} * [C \text{ uptake rate}_{\text{total}}] - \delta * Cb - D * Cb. \quad (6)$$

2.4. Equations for respiration

In addition to the acquisition of a C substrate (electron donor), bacterial respiration requires terminal electron acceptors (TEAs). Our model represents heterotrophic populations which can make a living from aerobic respiration, denitrification, and sulfate reduction, or a combination thereof, using O₂, NO₃⁻, and SO₄²⁻ as the TEA, respectively. The relative energetics of these metabolisms is incorporated into our growth equation (Eqn. (6)) through theoretical yield (Y_{theor} ; see Section 2.2). However, respiration must also depend on the availability and uptake kinetics of these compounds.

The rate of aerobic respiration (r_{O_2}) is defined (with units of mol-Ce C-mol biomass⁻¹ d⁻¹ where mol-Ce refers to moles of the oxidant respired in C equivalents) as:

$$r_{O_2} = \frac{\rho_{rO_2}}{\Theta_{O_2}} * \frac{O_2}{K_{rO_2} + O_2}, \quad (7)$$

where O_2 indicates the environmental concentration, and ρ_{rO_2} and K_{rO_2} denote the maximum uptake velocity and half-saturation constant for O₂ uptake, respectively. Θ_{O_2} is the molar ratio of O to C consumed during aerobic respiration.

In natural environments, O₂ is typically respired in advance of NO₃⁻, and SO₄²⁻ respiration happens only in the near-absence of both O₂ and NO₃⁻. This stepwise consumption occurs because of the relative energy yields of each reaction (Table B1). Ecologically, under aerobic conditions, obligate denitrifiers and sulfate reducers are outcompeted, and

facultative heterotrophs upregulate aerobic pathways. As our model describes a single metabolically flexible community, rather than explicitly resolving distinct metabolic communities and competitions between them, we account for this stepwise TEA utilization using inhibition terms based on the concentrations of O₂ and NO₃⁻ to calculate rates of denitrification (r_{NO_3}) and sulfate reduction (r_{SO_4}), respectively:

$$r_{NO_3} = \frac{\rho_{rNO_3}}{\Theta_{NO_3}} * \frac{Ne_{NO_3}}{K_{rNO_3} + Ne_{NO_3}} * \frac{\kappa_{rNO_3}^{O_2}}{\kappa_{rNO_3}^{O_2} + O_2^{\alpha_{rNO_3}}} \quad (8)$$

$$\text{and } r_{SO_4} = \frac{\rho_{rSO_4}}{\Theta_{SO_4}} * \frac{\kappa_{rSO_4}^{NO_3}}{\kappa_{rSO_4}^{NO_3} + (Ne_{NO_3} + O_2)^{\alpha_{rSO_4}}}, \quad (9)$$

where parameters κ and α in both equations regulate the sensitivity of r_{NO_3} and r_{SO_4} to O₂ and NO₃⁻ concentrations, respectively. Parameter κ defines the threshold at which O₂ or NO₃⁻ begins to inhibit the reactions, while α controls how sharply these inhibitions occur (Suppl. Fig. B1). In the denitrification equation, κ_{rNO_3} sets the oxygen threshold beyond which NO₃⁻ reduction is inhibited, while α_{rNO_3} determines how sharply this inhibition occurs. Similarly, in the SO₄²⁻ reduction equation, κ_{rSO_4} and α_{rSO_4} regulate the inhibition by both O₂ and NO₃⁻. This approach is representative of microbial downregulation of lower energy yield respiratory pathways in the presence of higher-yield TEAs, and stands in lieu of including active competition among obligate aerobes, denitrifiers, and SO₄²⁻ reducers.

As described in Section 2.3, a part of energy demand is allotted to supporting cellular maintenance processes without biomass growth ($m_{O_2} + m_{NO_3} + m_{SO_4}$). Maintenance respiration of NO₃⁻ (m_{NO_3}) and SO₄²⁻ (m_{SO_4}) are defined using the same equation forms as shown in Eqns. (8) and 9, respectively, with some varied parameters (see Section 2.6).

Under oxic conditions, N₂ fixation incurs an additional indirect energy cost, which is associated with protecting the nitrogenase enzyme from oxidative damage (Großkopf and LaRoche, 2012; Inomura et al., 2017). This cost is included by the second term of the aerobic maintenance respiration (m_{O_2}) equation:

$$m_{O_2} = \frac{\rho_{mO_2}}{\Theta_{O_2}} * \frac{O_2}{K_{mO_2} + O_2} + \frac{u_{N_2}}{u_{NH_4} + u_{NO_3} + u_{N_2}} * \frac{\rho_{mO_2}}{\Theta_{O_2}} * \frac{O_2}{K_{mO_2} + O_2}, \quad (10)$$

which increases proportionally with the fraction of N uptake associated with N₂ fixation to reflect the cost of N uptake. If we follow the diffusion of O₂, the respiratory cost may increase linearly with oxygen concentration. However, the data show non-linearly increasing cellular carbon consumption with increasing O₂ concentration (Kuhla and Oelze, 1988), possibly N₂ fixing cells physiologically adapting to increased O₂ concentration (Inomura et al., 2017; Post et al., 1982; Sabra et al., 2000). The saturating formula for O₂ is meant to reflect such effects. Section 2.6 describes the parameterization of these functions.

2.5. Equations for nitrogen utilization

To track the flow of different N sources into biomass, we considered the molar amount of N in biomass (Nb) as:

$$Nb = Nb_{NH_4} + Nb_{NO_3} + Nb_{N_2}. \quad (11)$$

Nb_{NH_4} , Nb_{NO_3} and Nb_{N_2} describes the biomass N that originates from subscribed N sources. The environmental concentration of NH₄⁺ (Ne_{NH_4}) and NO₃⁻ (Ne_{NO_3}) changes as described for C substrate concentration in Eqn. (5) (see Suppl. Text B2). The Nb regeneration is mostly added to the Ne_{NH_4} pool, with a small fraction supplying Ne_{NO_3} (assuming instantaneous ammonification and nitrification; see Suppl. Text B2).

Biomass derived from each respective N source (here, generalized as ‘x’ for simplicity) increases by uptake rate (u_x) bounded by $Q_{Nb,Cb}$, and decreases by biomass death (δ) and dilution (D) following the form:

$$\frac{dNb_x}{dt} = u_x * \frac{Q_{max} - Q_{Nb:Cb}}{Q_{max} - Q_{min}} * Cb - \delta * Nb_x - D * Nb_x. \quad (12)$$

The uptake rates (u) of the environmental NH_4^+ (Ne_{NH_4}), NO_3^- (Ne_{NO_3}), and N_2 (Ne_{N_2}) pools are interdependent such that NH_4^+ is preferentially assimilated, followed by NO_3^- , followed by N_2 :

$$u_{NH_4} = \rho_{uNH_4} * \frac{Ne_{NH_4}}{K_{uNH_4} + Ne_{NH_4}} \quad (13)$$

$$u_{NO_3} = \rho_{uNO_3} * \frac{Ne_{NO_3}}{K_{uNO_3} + Ne_{NO_3}} * \frac{\kappa_{uNO_3}^{\alpha_{uNO_3}}}{\kappa_{uNO_3}^{\alpha_{uNO_3}} + \left(\frac{Nb_{NH_4}}{Cb}\right)^{\alpha_{uNO_3}}} \quad (14)$$

$$u_{N_2} = \rho_{uN_2} * \frac{\kappa_{uN_2}^{\alpha_{uN_2}}}{\kappa_{uN_2}^{\alpha_{uN_2}} + \left(\frac{Nb_{NH_4} + Nb_{NO_3}}{Cb}\right)^{\alpha_{uN_2}}}. \quad (15)$$

As described in Section 2.4, κ values define the threshold concentration at which an N uptake pathway is downregulated, while α controls how sharply these inhibitions occur.

2.6. Model parameterization

Our aim in crafting this model was to represent a population of aquatic, heterotrophic diazotrophs to investigate drivers of their activity across environmental gradients. However, relatively little physiological data is available on heterotrophic diazotrophs, either from culturing studies or the environment, for parameterization of stoichiometric and kinetic constraints in our model. (Thermodynamic constraints did not require comparable literature parameterization; see Section 2.2.) To assess the range of available data, we first performed a literature search using *Web of Science*. We began our search by focusing specifically on *Azotobacter vinelandii*, a model heterotrophic diazotroph that has long been in culture and whose physiology is well-studied. This makes *Azotobacter vinelandii* distinct as few heterotrophic diazotrophs from aquatic environments have ever been identified to species-level, and far fewer have been successfully isolated from aquatic systems. The specific search terms were: (Azotobacter vinelandii) AND (cult* OR lab*) AND (carbon OR nitrogen OR stoich*), resulting in 385 total papers on August 22, 2023. Of these, 15 papers fit our criteria of containing relevant physiological data for *A. vinelandii* in culture or lab-based environments that were relevant to our parameter needs. If raw data were not available, values were manually extracted from tables and figures using PlotDigitizer (<https://plotdigitizer.com/>). Data were collated across all studies to determine parameter values for the model and establish maximum and minimum values for sensitivity analysis. For parameters with no available data for *A. vinelandii*, we broadened a literature search to find sources from other heterotrophic bacteria, prioritizing data from specifically aquatic organisms where available. To determine the values of Q_{min} and Q_{max} , we used the range of molar N:C biomass reported across heterotrophic bacteria (Godwin and Cotner, 2015). Parameters were selected from the range of available literature and, due to the limitations of this pool, were not screened based on temperature or pH; however, where possible, we worked to cover a range of relevant environmental conditions such that this variability would be accounted for when performing our sensitivity analysis (Section 2.7; 3.5). A full description of model parameterization can be found in Supplement B (Text B3), including how baseline values for the model were selected. All resulting model parameters values are summarized in Suppl. Table B1 and a complete version including minimum and maximum values is available in machine-readable format as Supplement C. See Section 2.9 for discussion on limitations of the approach.

We selected a fixed value of 3 for all the α parameters in our model to ensure a smooth yet responsive transition around the κ thresholds (Suppl. Fig. B1). This choice balances a sharp enough reaction to changes in substrate concentration without causing abrupt, unrealistic

shifts in the dependent uptake rates. Regarding the κ threshold values for NO_3^- uptake and N_2 fixation, these values have not been directly quantified in the literature. We chose values to represent cellular N:C quotas that were within the range of Q_{min} and Q_{max} and approximated cellular N:C quotas at which N-limitation could trigger NO_3^- uptake or N_2 fixation.

2.7. Sensitivity analysis

We explored the relative importance of different physiological parameters, including selected α and κ values, on model outputs with a global parameter sensitivity analysis using Latin Hypercube Sampling (LHS), a stratified Monte Carlo sampling technique that allows for unbiased selection of parameter values (Marino et al., 2008). We used the realized yield, biomass, and proportion of cellular N derived from N_2 fixation as output measures and explored the influences of parameters ranging between values listed in Suppl. Table D1. We verified that the parameters have monotonic relationships with the model output measures, suggesting the Partial Ranked Correlation Coefficient (PRCC) is an appropriate statistical measure (Suppl. Figs. D1–5). We conducted z-tests on the PRCC values to rank them by importance.

2.8. Scenarios to test model performance

The model was tested under five relevant environmental scenarios (Table 2) using (separately) acetate and glucose as the C substrate. Scenario 1 had relatively high (250 μM) concentrations of O_2 in the inflow, typical of waters in contact with the atmosphere at $\sim 25^\circ C$, and moderate organic C concentrations (200 μM) (Münster, 1993), with low inorganic nitrogen concentrations (0.1 μM NH_4^+ and 3 μM NO_3^-), which may favor N_2 fixation. Such conditions are representative of the euphotic zone of many tropical to temperate estuaries or coastal waters in summertime where N can become limiting and significant N_2 fixation is observed (e.g., Selden et al., 2024). Scenario 2 was identical to Scenario 1 but with higher fixed N concentrations (1 μM NH_4^+ and 30 μM NO_3^-) more typical of a mesotrophic lake or river (Durand et al., 2011). Scenarios 3–5 had low O_2 resupply rates (25 μM) to force anaerobic metabolism. Scenario 3 was otherwise identical to Scenario 2, representing an N-replete O_2 deficient zones such as those observed at ocean margins or seasonally in impacted estuaries (e.g., Dodds, 2006); Scenario 4 represented an N-deplete O_2 deficient zone as may be found in deep waters of a highly stratified lake or fjord (e.g., Pawlowicz et al., 2007). Finally, in Scenario 5, concentrations of organic C and NH_4^+ were increased to 2000 μM and 100 μM , respectively, representing eutrophic reducing sediments (Burdige and Zheng, 1998). Initial C biomass was 1 μM and the chemostat dilution rate was 0.1 d^{-1} across all scenario runs. Numerical simulations were produced using MATLAB version 9.13. For Figs. 3–4 and Suppl. Fig. 2B, steady state values were calculated as mean from days 50–60. To assess the validity of our model results, we

Table 2
Environmental scenarios under which model was tested.

Scenario	Simulated environment	Inflow concentrations			
		C source (μM)	NH_4^+ (μM)	NO_3^- (μM)	O_2 (μM)
1	Coastal ocean/estuary, upper water column	200	0.1	3	250
2	Mesotrophic lake/river, water column	200	1	30	250
3	Mesotrophic estuary, suboxic bottom waters	200	1	30	25
4	N-limited lake/river/estuary/fjord, suboxic bottom waters	200	1	3	25
5	Eutrophic reducing sediments	2000	100	30	25

compared our findings to both culturing and field data omitted from model parameterization (see Section 3.5).

2.9. Model limitations

The model presented investigates N and C lability, availability, and stoichiometry as drivers of heterotrophic diazotrophy. We note that, in aquatic systems, both phosphorus and iron availability commonly limit diazotrophic growth; however, these variables, while important, were beyond our scope. Additionally, our GEDM approach to constraining bacterial energetics does not account for several additional costs such as uptake transporters, enzyme synthesis, or enzyme activation energy inputs (see Section 4.1 for further discussion).

To overcome the low availability of relevant data, parameters were sourced from both culturing data (where available) and environmental data, and included a range of heterotrophic bacteria and environment types (see Section 2.6 and Suppl. Text B3 for description of parameter selection). While unavoidable, this approach introduces a major model limitation: Because diazotroph physiology may differ from that of (aquatic) heterotrophs more generally, and likely differs among diazotrophs which inhabit distinct environment types, our middle-of-the-road baseline parameter set may not effectively represent all heterotrophic diazotrophs under all environmental conditions. Nevertheless, the model effectively replicates environmental observations across diverse environments (Section 3.5). This approach also presented the opportunity to assess which parameters were most impactful to model output under different environmental scenarios (Section 3.6) which, we hope, can help guide future culturing work.

3. Results

3.1. Theoretical yields

Our theoretical yield calculations, which consider strictly the relative thermodynamics of metabolic processes (Eqn. (1); Fig. 2A) and do not include respiratory protection of nitrogenase, demonstrate that the differences in the direct energetic cost (i.e., reduction and assimilation) among N sources have a small effect on growth yield compared to that associated with different C sources or TEAs. Theoretical growth yields under aerobic standard conditions were <10 % lower when growing on N_2 versus NH_4^+ , and only ~2 % lower than NO_3^- assimilation. In contrast, theoretical yield associated with aerobic respiration of acetate, and anabolism of acetate and ammonium, are 32.6 % lower than those associated with glucose utilization. Similarly, when glucose and NH_4^+ are

the C and N sources, respectively, theoretical yields during SO_4^{2-} reduction are 65 % lower than those associated with aerobic respiration. These substantial differences are consistent with an expectedly large decrease in fitness when O_2 and labile C sources are depleted.

3.2. Scenarios 1–2 (aerobic) and the effects of O_2

In addition to the direct cost of growth accounted for in the theoretical yield calculation, realized yield incorporates the cost of basal metabolism and indirect costs associated with N_2 fixation i.e., increased respiration to prevent oxidative damage to the nitrogenase complex. Across all scenarios, glucose resulted in higher realized yields and C-biomass concentrations than acetate at steady-state (calculated as mean from days 50–60) (Suppl. Table B1; Fig. 3A-D), as expected based on energy available from catabolism (Table 1). The maximum realized yield (0.39) was observed in Scenario 2, under anoxic atmosphere and with NH_4^+ (1 μM) and NO_3^- (30 μM) in the inflow (Table 3). This scenario represents a warm, mesotrophic water column such as may be found in tropical to temperate lakes, rivers and some estuaries where N_2 fixation rates are, in some cases, observable despite the trophic state (e.g., Bentzon-Tilia et al., 2015b; Scott et al., 2009). C-biomass concentration at steady-state was 73 μM . In contrast, C-biomass reached only 49 μM in Scenario 2, with acetate as the C source. The majority of N demand in both Scenario 2 cases was met by uptake of NO_3^- , which remained abundant in solution (Suppl. Fig. B2E-F), with a negligible fraction (<5 %) coming from NH_4^+ and N_2 combined (Suppl. Fig. B2 G-H, Table B1). This observation, in combination with the observation that media concentrations of acetate and glucose, respectively, dwindled to negligible levels within a week (Suppl. Fig. B2A-B), demonstrates that C-limitation was achieved in Scenario 2 regardless of C source.

In contrast, N_2 fixation represented a much larger portion of the N demand in theoxic, low-N scenario (Scenario 1; 0.1 μM NH_4^+ and 3 μM NO_3^- ; Fig. 3E-F) representative of conditions common in the upper water column of estuarine and coastal waters in the late spring/summer after nutrients from winter mixing have been drawn down. In the first week of growth, NO_3^- was the major N form (Suppl. Fig. B2E-F), with the relative importance of N_2 fixation increasing steadily (Fig. 3E-F) until it reached its maximum—about 63 % and 72 % for acetate and glucose trials, respectively. The additional N demand associated with higher growth in the glucose trial was met through N_2 fixation. As in Scenario 2, C availability was the factor which ultimately limited growth.

The evidence of near-complete C source consumption under both scenarios is further emphasized by changes in C-biomass/N-biomass ratio (Fig. 3G-H), which in all cases increases immediately upon model

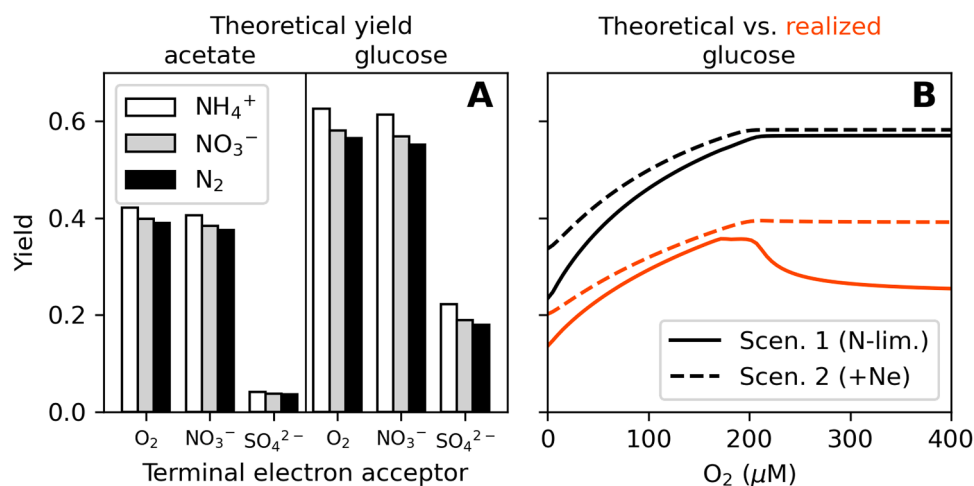


Fig. 2. (A) Calculated theoretical growth yields for combinations of respiratory electron donors, electron acceptors, and nitrogen sources, and theoretical (black) and realized (red) yields for growth on acetate (B) or glucose (C) observed over a range of steady-state O_2 concentrations under N-limited (Scenario 1; solid lines) and fixed N-replete (Scenario 2; dashed lines) conditions.

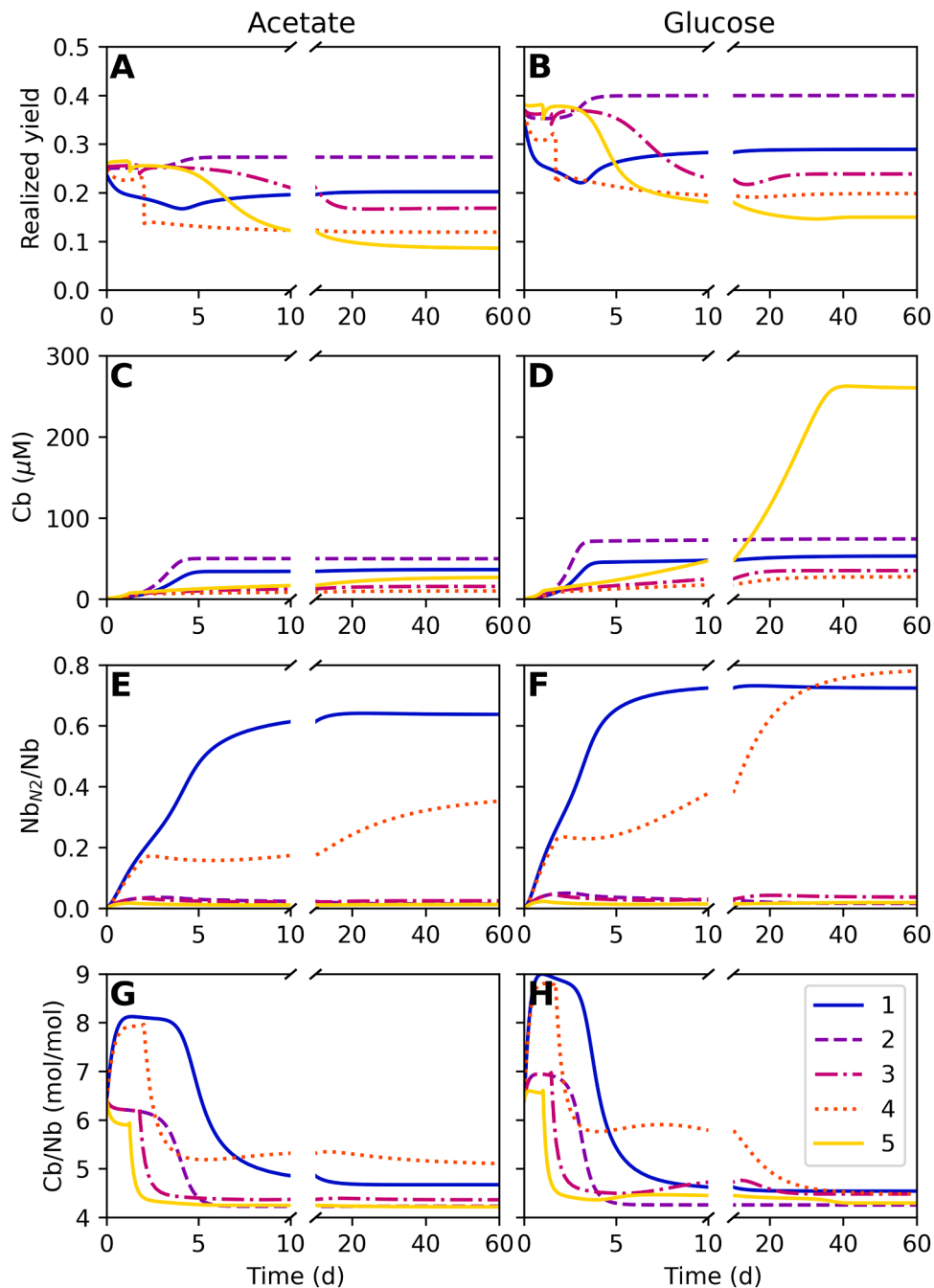


Fig. 3. Results of scenarios 1–5 through time with acetate (A, C, E, G) or glucose (B, D, F, H) as the carbon source: (A–B) realized yield, (C–D) carbon in biomass (Cb; μM), (E–F) the proportion of nitrogen in biomass (N_b) derived from N_2 fixation, and (G–H) realized yield i.e., carbon incorporated into biomass as a proportion of total carbon uptake.

initialization then falls around day 5 as the C substrate concentration in the environment reaches its steady-state minimum. The biomass C/N ratio maximum is highest in Scenario 1 (low fixed N availability) with glucose as the C source, due to the higher burden of assimilating N_2 -derived N and the greater realized yield associated with glucose. The steady-state (minimum) biomass C/N ratio was slightly lower in Scenario 2 than Scenario 1 where NO_3^- remained available (Suppl. Fig. B2E–F).

To assess the relative importance of the indirect respiratory cost of protecting nitrogenase from N inhibition, we ran Scenarios 1 (N-limited) and 2 (N-replete) to steady-state (100 d), varying O_2 concentrations (Fig. B3B). Realized yields under Scenario 1 conditions, where generally >65 % of the N demand was met by N_2 fixation (Suppl. Fig. B3A,C),

decreased rapidly at low steady-state O_2 concentrations (<20 μM , or 0.62 mg L^{-1}). Regardless of C source, realized yields in Scenarios 1 and 2 differed by <20 % in this range and by <10 % when O_2 concentrations were <5 μM (Suppl. Fig. B3B,D). Above 200 μM , realized yields under N-limited and N-replete conditions differed by >35 % (Fig. 2B; Suppl. Fig. B3C,D) with N_2 fixation activity slowly declining with increasing O_2 concentration in Scenario 1 (Suppl. Fig. B3A,B) as the increasing energy burden decreased growth rates.

3.3. Scenarios 3–4 (anaerobic) and the effects of C substrate richness

Scenario 3, representative of the bottom waters of a mesotrophic estuary, was comparable to Scenario 2 in terms of its nutrient

Table 3Results of sensitivity analysis for realized yield, biomass, and proportion of cellular N derived from N₂ fixation¹.

Variable/ Scenario	Parameter									
	TheorY	K _m *	ρ _{m2O2} *	ρ _{m1O2} *	Q _{max}	Q _{min}	ρ _{rO2}	K _r	K _{m1O2} ²	K _{rSO4}
Realized Yield										
1	1 (0.84)	2 (0.70)	3 (-0.62)	4 (-0.33)	5 (0.21)	6 (-0.07)	6 (-0.08)			
2	1 (0.84)	2 (0.70)	3 (-0.60)	4 (-0.36)	5 (0.23)	6 (-0.12)	6 (-0.09)			
3	1 (0.84)	2 (0.63)	3 (-0.54)	3 (-0.56)	5 (0.16)		6 (-0.15)		4 (0.33)	
4	1 (0.84)	2 (0.64)	3 (-0.51)	3 (-0.53)	5 (0.17)		6 (-0.16)		4 (0.31)	
5	1 (0.86)	2 (0.48)	3 (-0.40)	3 (-0.41)	5 (0.27)				4 (0.40)	
Cb										
1	1 (0.80)	3 (0.50)	4 (-0.44)	7 (-0.18)	6 (0.29)	8 (-0.12)	2 (0.52)	5 (-0.37)		
2	1 (0.79)	3 (0.48)	4 (-0.40)	7 (-0.20)	6 (0.29)	8 (-0.16)	2 (0.53)	5 (-0.35)		
3	1 (0.76)	2 (0.39)	3 (-0.37)	3 (-0.39)	6 (0.23)	7 (-0.09)	4 (0.31)	5 (-0.27)	6 (0.23)	
4	1 (0.76)	2 (0.38)	3 (-0.33)	3 (-0.33)	5 (0.22)	6 (-0.09)	4 (0.31)	3 (-0.33)	5 (0.20)	
5	1 (0.83)		4 (-0.35)	4 (-0.34)	6 (0.31)			2 (-0.49)	5 (0.34)	3 (0.37)
Nb_{N2}										
1	1 (0.78)	4 (0.47)	5 (-0.40)	7 (-0.16)	2 (0.56)	8 (-0.11)	3 (0.51)	6 (-0.35)		
2	1 (0.78)	4 (0.44)	5 (-0.36)	6 (-0.18)	2 (0.56)	7 (-0.14)	3 (0.51)	5 (-0.34)	7 (0.20)	
3	1 (0.75)	3 (0.36)	4 (-0.34)	4 (-0.36)	2 (0.53)	8 (-0.06)	5 (0.31)	6 (-0.27)		
4	1 (0.74)	3 (0.37)	5 (-0.30)	5 (-0.31)	2 (0.52)	7 (-0.07)	4 (0.31)	5 (-0.32)	6 (0.18)	
5	1 (0.82)		5 (-0.33)	5 (-0.32)	2 (0.59)			4 (-0.48)	6 (0.32)	3 (0.37)

¹ The table lists the ranking from 1 to 8 of the most influential physiological parameters on the realized yield, biomass *Cb*, and proportion of cellular N derived from fixation N_{b-N2} across all five scenarios. The corresponding PRCC values for each ranking are given in parentheses.

² Parameter values were varied between dynamic ranges using factors, see Appendix D for more information.

concentrations (high fixed N; Table 3), but the O₂ inflow concentration was low (25 μM), resulting in suboxic conditions that forced denitrification (Fig. 4C-D) and then sulfate reduction (Fig. 4E-F). Such conditions commonly occur during the summer when increased stratification and productivity can create seasonal O₂ deficiency (Testa et al., 2018). After O₂ concentrations were rapidly drawn down (Fig. S1A-B), denitrification ramped up and then decreased as more total NO₃ was allotted to assimilatory processes (Suppl. Fig. B4) and SO₄²⁻ reduction rates increased (Fig. 4).

In Scenario 4, representative of suboxic bottom waters or sinking particles where fixed N had been drawn, inflow NO₃ concentration was lowered by an order of magnitude (to 3 μM), which caused the energy cost of anabolism to increase (given the greater reliance on N₂; Fig. 3E-F) and the energy yield of catabolism to decrease (given the greater reliance on SO₄²⁻ reduction; Fig. 4A-F). This decreased realized yield by 30 % (from 0.17 in Scenario 3 to 0.12) in the acetate trial and 17 % (from 0.23 to 0.19) in the glucose trial with roughly equivalent declines in steady-state C-biomass (Suppl. Table B1; Fig. 3A-D). Over the course of the model run, the glucose-respiring community shifted from growing primarily on NO₃ to N₂ fixation. At model initialization, NO₃ and NH₄⁺ assimilation accounted for 75 % and 25 % of N demand, respectively (Suppl. Fig. B4); by day 60, N₂ fixation represented 78 % of N demand, similar to Scenario 1 (Fig. 3F). As growth rates were lower in the acetate trial, NO₃ continued to satiate a large proportion of N demand throughout the run (47 % by day 60; Suppl. Fig. B4), with N₂ fixation accounting for only 35 % by day 60—a value nearly half that achieved in the Scenario 1 simulation with acetate (Fig. 3E).

Our findings show that the community cost of living under suboxia is minimized when a more energy-rich C substrate is available. Overall, the switch from aerobic (Scenario 2) to anaerobic (Scenario 3) metabolism decreased steady-state realized yields by ~40 % and biomass by more than half in both acetate and glucose trials (69 % for acetate and 53 % for glucose; Suppl. Table B2). However, growth rates on glucose, a more energy-rich molecule, under suboxic conditions in Scenario 3 were more than twice those on acetate; under oxic conditions in Scenario 2, glucose yielded only 1.5x higher growth rates than acetate (Suppl. Table B2). Regardless of C source, the C substrate was never completely drawn down in Scenarios 3 and 4, reaching ~100 μM at steady-state (Suppl. Fig. B2A-B). NO₃ similarly remained above 3 and 5 μM in acetate and glucose trials, respectively (Suppl. Fig. B2E-F), and N₂ fixation remained a small component of total N demand. Growth was thus constrained by the relative kinetics of C and N uptake and the sensitivity of N₂ fixation

to Ne, with NO₃+NH₄⁺ concentrations too low to be used efficiently but too high to trigger N₂ fixation and C concentrations too low to support N₂ fixation even in the absence of O₂. Parsing the importance of diazotroph trait variability as a control of N₂ fixation is beyond the scope of this report, but of probable significance and, consequently, good fodder for future work.

C substrate energy yields (i.e., energetic richness) affected whether oxic or suboxic conditions were most conducive to N₂ fixation. While growing on acetate, a less energy-rich molecule than glucose, Scenario 1 (oxic, N-limited) supported more diazotrophy at steady-state than Scenario 4 (suboxic, N-limited), regardless of metric (Suppl. Table B2). However, during growth on glucose, rates of N—N₂ assimilation normalized per mole C-biomass, as well as the proportional importance of N₂ to total N demand, were maximized in Scenario 4 (Fig. 3E-F; Suppl. Table B2). Absolute rates (on a per volume basis, as most environmental measurements are presented) were highest in Scenario 1 regardless of C source (Suppl. Table B2). Nevertheless, during growth on glucose, absolute N₂ fixation rates for Scenario 4 were of the same magnitude as those in Scenario 1.

3.4. Scenario 5 (eutrophic, anaerobic) and the effects of exogenous N

In Scenario 5, organic C and NH₄⁺ inflow concentrations were increased to 2000 μM and 100 μM, respectively, representing eutrophic and highly reducing aquatic sediments (Table 3). Such conditions may be found in organic-rich depositional environments like wetlands, salt marshes, tidal flats, or mangrove/seagrass sediments, where areal N₂ fixation rates can be on par with or exceed overlying waters (Fulweiler et al., 2025). Here, denitrification rates followed similar patterns to Scenario 3 (Suppl. Fig. B2C-D), while sulfate reduction rates rose somewhat more slowly (Fig. 4E-F). NO₃ concentrations and the proportion of N demand met by NO₃ decreased from nearly 50 % on day 2 to only 15 % and 4 % by day 60 in the acetate and glucose trials, respectively (Suppl. Figs. B2, B4). NH₄⁺ uptake accounted for most of the residual N demand, with N₂ fixation supply only ~1–2 % of N at steady-state (Fig. 3E-F).

We found that, while growing on glucose, exceptionally high biomass was achieved under Scenario 5 conditions (Fig. 3D) despite reliance of the community on sulfate respiration (Fig. 4F; Suppl. Table B2), driving notable absolute N₂ fixation rates (Fig. 4H) in the presence of exogenous NH₄⁺ (>35 μM at steady-state; Suppl. Fig. B2H). Steady state realized yields were exceptionally low in both acetate

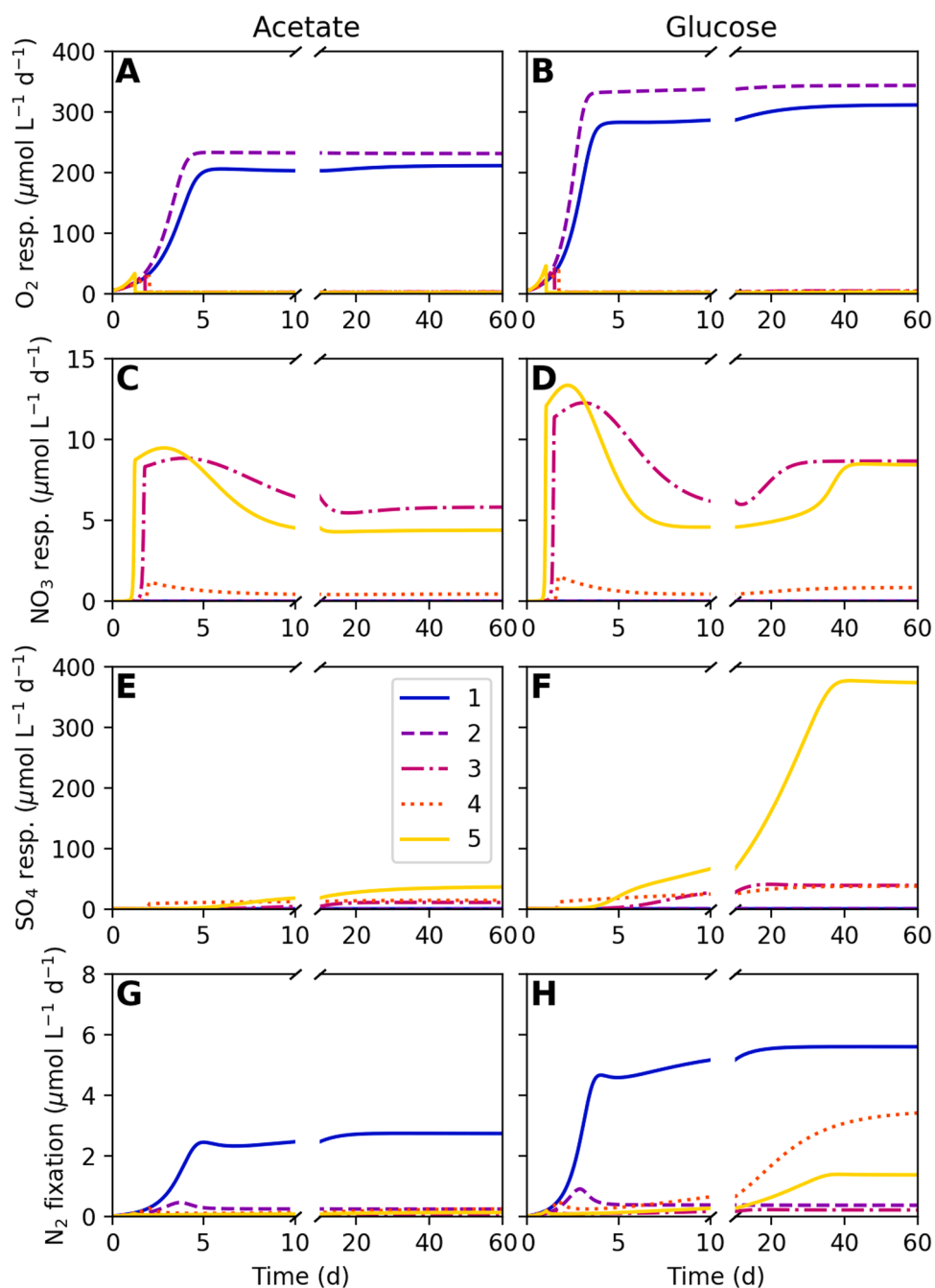


Fig. 4. Results of scenarios 1–5 through time with acetate (A, C, E, G) or glucose (B, D, F, H) as the carbon source: (A–B) aerobic respiration rate ($\mu\text{mol O}_2 \text{ L}^{-1} \text{ d}^{-1}$), (C–D) denitrification rate ($\mu\text{mol NO}_3 \text{ L}^{-1} \text{ d}^{-1}$), and (E–F) sulfate reduction rate ($\mu\text{mol SO}_4^{2-} \text{ L}^{-1} \text{ d}^{-1}$), and N_2 fixation rate ($\mu\text{mol N}_2 \text{ L}^{-1} \text{ d}^{-1}$).

(0.09) and glucose (0.15) Scenario 5 trials (Fig. 3A–B); nonetheless, in the glucose trial, high sulfate respiration rates (Fig. 4F) drove C-biomass concentrations up to $260 \mu\text{M}$ at steady-state, where environmental C concentrations leveled out at $117 \mu\text{M}$ (Fig. 3D; Suppl. Table B2). This value is 3.5x greater than the C-biomass achieved under oxic, N-replete conditions with $200 \mu\text{M}$ glucose in the feedstock ($73 \mu\text{M}$ in Scenario 2). As SO_4^{2-} respiration rates and C-biomass rose rapidly between days 10 and 40, absolute rates of N_2 fixation rose with them (Fig. 3D; Fig. 4F, H), reaching $1.38 \mu\text{mol L}^{-1} \text{ d}^{-1}$ at steady-state (Suppl. Table B2). This value is of equal magnitude with absolute N_2 fixation rates observed in oxic (Scenario 1) and suboxic (Scenario 4) N-deplete glucose trials (Fig. 4H).

The relative sensitivity of N_2 fixation to exogenous N was also lower under Scenario 5 conditions with glucose than in other trials. To investigate environment C and N stoichiometry on N_2 fixation rates, we

varied $N_{e\text{NH}_4}$ relative to organic C concentrations. Under Scenario 5 conditions with glucose, the relative contribution of N_2 to total N demand rose with decreasing environment N (NH_4^+ plus NO_3^-) concentrations, reaching $>4\%$ where the steady-state in situ concentration of fixed N was $10 \mu\text{M}$ and $>10\%$ below $4 \mu\text{M}$ (Fig. 5A). The relative utilization of N_2 was reduced in Scenario 2 (oxic) and 3 (suboxic) runs—which had an order of magnitude lower concentrations of glucose and NO_3^- , and in runs with acetate as the C source. This diminished sensitivity occurred despite use of identical “on/off switches” in all trials (see Section 2.4). In Scenarios 2, 3, and 5, the relative importance of N_2 fixation increased with C/N of environmental substrates (Fig. 5B); the rate of this increase was greater for growth on glucose than acetate, and scaled identically in both Scenarios 3 and 5, indicating that the relationship is independent of substrate concentrations in the environment.

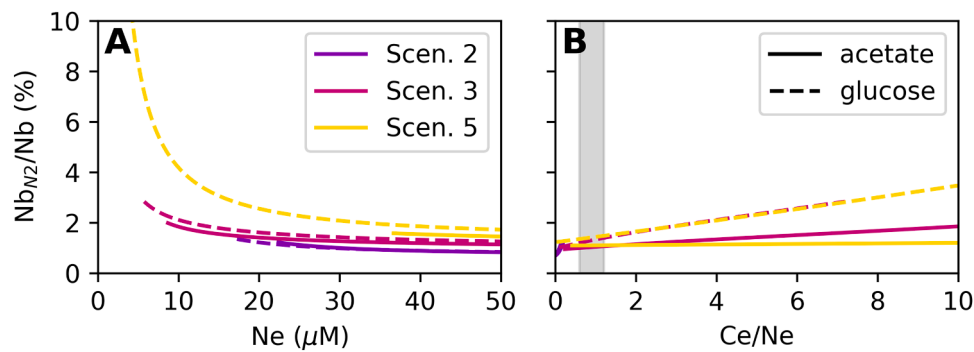


Fig. 5. The proportion of biomass N derived from N_2 fixation (Nb_{N_2}/Nb) at steady-state ($t = 100$ d) as a function of the steady-state concentration of fixed N in the environment (Ne i.e., the sum of NH_4^+ and NO_3^- concentrations (A) and the molar ratio of labile C to N in the environment (Ce/Ne on a logarithmic scale; B) in Scenarios 2 (purple), 3 (pink), and 5 (yellow); solid and dashed lines indicate acetate and glucose trials, respectively. Concentrations of constituents in the inflow are as given for each scenario in Table 2 except for ammonium, which was varied to achieve Ce/Ne ratios from 0 to 50 in the chemostat inflow. The shaded region shows the range of allowable microbial stoichiometry in the model (i.e., the range between Q_{min} and Q_{max}).

3.5. Model assessment

Our model output is in keeping with the results of laboratory studies which were not included in model parameterization. Post et al. (1983) measured aerobic respiration rates in *A. vinelandii* in culture of 20–188 mol O/mol C in biomass/day using a high dilution rate (0.15 h^{-1}) and a high organic C concentration in the inflow (110,000 to 525,000 μM) Steady-state respiration rates predicted by our model under aerobic conditions (Scenarios 1 and 2) using an organic C concentration of relevance to aquatic systems (200 μM ; see Section 2.8) were lower, as expected, but within an order of magnitude, ranging from 9.4 to 12.1 mol O/mol C in biomass/day (Suppl. Table B2). In a recent synthesis of work on *A. vinelandii*, Castillo et al. (2020) report aerobic respiration rates ranging from 2.8–218 mol O/mol C in biomass/day, which encompasses our values. Similarly, the range of steady state N_2 fixation rates observed across our modeled scenarios (4.9 – 130 mmol N / mol C in biomass / day; Suppl. Table B2) was lower than Post et al. (1983; 507 – 1608 mmol N / mol C in biomass / day) under N-starved conditions; this is, again, an expected discrepancy given the differences described above as well as fixed N in model inflow.

Our model results are also broadly in keeping with environmental observations. Our absolute N_2 fixation rates in eutrophic and reducing sediments (Scenario 5) were 0.13 and 1.38 $\mu\text{mol N L}^{-1}\text{ d}^{-1}$ with acetate and glucose as the C source, respectively (Suppl. Table B2). These values fall squarely within the range of measurable rates observed in comparable benthic systems (salt marshes, mangroves, seagrasses, tidal flats, estuaries): 0.10 – 42 $\mu\text{mol N L}^{-1}\text{ d}^{-1}$ (Fulweiler et al., 2025). Predicted N_2 fixation rates under N-limiting conditions in oxic (Scenario 1) and suboxic (Scenario 4) water columns ranged from 0.25 (with less labile C source under oxic conditions) to 5.61 $\mu\text{mol N L}^{-1}\text{ d}^{-1}$ (with glucose under oxic conditions). While these values are of similar magnitude to culturing studies (see above), they are high relative to environmental observations. For example, Pedersen et al. (2018) observed rates $<0.22\text{ }\mu\text{mol N L}^{-1}\text{ d}^{-1}$ in estuarine waters with resuspended sediments. This difference likely reflects the complexity and lower average lability of environmental organic C compounds relative to acetate or glucose, and the omission of other limiting factors (e.g., phosphorus or iron) represented in our model.

3.6. Sensitivity analysis

The most sensitive parameters in the model were ranked from 1–6 for realized growth yield (Y_{real}), C-biomass (Cb), and the proportion of N demand met by N_2 fixation (Nb_{N_2}) across each of the five different scenarios by comparing their PRCC values (Table 3). Ranging between -1 to 1 , PRCC values (shown for each parameter in each scenario in parentheses) with the greatest magnitude were the most influential,

where the sign denotes correlational direction. PRCC values close to zero have minimal effects. Theoretical growth yield (Y_{theor}), which is derived per reaction set from ΔG values (see Section 2.2), was varied as a parameter in sensitivity analysis; it was the most sensitive parameter controlling all three model outputs regardless of the scenario. However, other parameters appeared to be consistently important. For example, the half-saturation constant for C substrate uptake (K_m) and the maximum O_2 uptake rates for respiration supporting basal metabolism (ρ_{mO_2}) and nitrogenase protection (ρ_{mNO_2}) were consistently ranked the second to fourth most influential parameters in controlling realized yield regardless of the modeling scenario. In keeping with these observations, Cb was strongly controlled by the maximum O_2 uptake rate for respiration supporting biosynthesis (ρ_{rO_2}) in Scenarios 1 and 2, K_m in Scenarios 3 and 4, and the half-saturation constant for growth-associated C uptake (K_r) in Scenario 5. Notably, the maximum $Nb : Cb$ ratio (Q_{max}) was consistently the second most sensitive parameter when modelling the proportional contribution of N_2 fixation to N demand, regardless of scenario, but Q_{min} was never ranked highly for any variable in any scenario. These results indicate that parameters related to energy acquisition and respiratory efficiency tended to be the most sensitive compared to parameters related to nutrient acquisition or regulation. For further details on the sensitivity analysis, including parameter ranges and values plots showing output changes as functions of each parameter, please see Supplement D.

4. Discussion

4.1. C (and not N) source drives thermodynamic efficiency of growth

Microbes are open thermodynamic systems which couple energy and mass flow to drive replication and produce entropy (Calabrese et al., 2021). The ability of a microbial community to effectively harness energy from its environment is as fundamental a constraint on growth as the accessibility of assimilable mass. This thermodynamic efficiency (Penocchio et al., 2019) depends on the energy yields of catabolism (ΔG_{cat}) relative to the cost associated with anabolism (ΔG_{ana}) and associated free energy loss through dissipation (in accordance with the second law of thermodynamics; ΔG_{diss}), described in C units here as theoretical yield (Eqn. (1)). In our heterotroph model, both energy and mass requirements for growth are met by the C substrate. Growth in our model is not dependent on energy stored in the bonds of the N species consumed to meet N mass requirements. Thus, unlike C substrate form, which affects all three terms, N substrate form factors only into the cost of growth.

To compare the impact of N substrate form on energetics, we must first consider more specifically where costs lie. The costs of N_2 fixation are multifold, variable, and the subject of prior review (see Gutschick,

2005; Pate et al., 1990). The major direct costs of N_2 fixation are [1] reducing N_2 to NH_4^+ and [2] reducing protons to H_2 . Both direct expenses [1] and [2], as well as the overall cost of biosynthesis, are considered in the model presented here within the thermodynamic cost of N_2 assimilation (Table 1). Nitrogenase obligatorily reduces protons even while fixing N_2 (Gutschick, 2005), with an estimated ratio of 0.65 mol H_2 per 1 mol NH_4^+ produced under a natural atmosphere (Andersen and Shanmugam, 1977). However, the realized cost of this additional reduction may be minimized by expression of an uptake hydrogenase (Hup), which reduces the loss by reoxidizing nitrogenase-generated H_2 (Pate et al., 1990; Stam et al., 1987); our model does not consider this cost-saving mechanism. Indirect costs of N_2 fixation include [3] capital energy investment in enzyme synthesis, [4] maintenance costs associated with protein turnover, and [5] protection of nitrogenase from O_2 inhibition in oxic environments (Gutschick, 2005). We include an additional respiratory burden associated with [5] as well as basal metabolism in calculating realized yield, but do not explicitly consider [3] or [4] or the costs associated with active transport of NO_3^- and NH_4^+ ions into the cell, though these costs are implicitly considered in bulk as a part of basal metabolism.

Our theoretical yield calculations (Eqn. (1); Fig. 2A) show that the differences in the direct energetic cost (i.e., reduction and assimilation) among N sources are small but can be substantial when considered in the context of net metabolism. Previous work (see reviews by Gutschick, 2005; Pate et al., 1990) has calculated the costs of assimilating different N sources directly. Comparing simply the cost of reduction, (Falkowski, 1983) calculated that N_2 ($\Delta G = 364 \text{ kJ mol}^{-1} NH_4^+$) requires $\sim 20\%$ more energy than NO_3^- ($\Delta G = 289 \text{ kJ mol}^{-1} NH_4^+$) [though this comparison depends on the exchange rate between intracellular currencies (ATP: NADPH) which is more favorable with a labile carbon source and high respiratory efficiency (Großkopf and LaRoche, 2012)]. Including the additional cost of proton reduction ($\Delta G = 39.9 \text{ kJ mol}^{-1} NH_4^+$) gives a $\sim 29\%$ greater energy cost. This difference is surely significant; yet, when we incorporate it into our Gibbs energy dissipation model (Table 1), which considers only the relative thermodynamics of catabolism/anabolism, the effective difference in aerobic growth yields between the different N sources (calculated as C incorporated into biomass as a proportion of total C uptake) is only $\sim 10\%$ (Fig. 2A). In contrast, aerobic respiration with glucose as the C source results in growth yields $>30\%$ greater than that with acetate (Fig. 2A). This result shows that, in the absence of major indirect costs associated with N_2 fixation (e.g., respiratory protection), N source is of lesser importance in determining growth efficiency than other factors, particularly C substrate energy yield.

4.2. Indirect costs of N_2 fixation are minimized under moderate O_2 concentrations

The importance of N_2 as an N source in our model depends on a tradeoff between the indirect cost of O_2 inhibition and the energy yield from favorable terminal electron acceptors. Our realized yield calculations (Eqn. (2)) show how the additional cost associated with protecting nitrogenase from oxidative stress (here, taken as increased respiration) on realized growth yield declines from $>35\%$ at $>200 \mu M O_2$ (typical of surface waters $<28^\circ C$ or $<25^\circ C$ for fresh and marine systems, respectively) to $<10\%$ under suboxic conditions ($<5 \mu M O_2$; Fig. 2B,C; Suppl. Fig. B3C,D). These values represent a minimum impact of O_2 on diazotrophic growth as they are derived from Scenario 1 simulations (see Section 3.2) in which there is a small but continuous influx of fixed N and, consequently, only 65–80 % of N biomass is derived from N_2 (Suppl. Fig. B3). Such conditions (low fixed N influx, ample organic C) are broadly representative of coastal and estuarine waters, which often experience variable O_2 concentrations seasonally, and can be met across seasonal and latitudinal gradients depending on local conditions.

While this model exclusively represents heterotrophic diazotrophs, modeled results are in good agreement with empirical work on the

cyanobacterium *Crocospaera* that has demonstrated that the indirect expense of protecting nitrogenase from oxidative stress represents a majority of the total cost of N_2 fixation at $186 \mu M O_2$, while at $46 \mu M O_2$ the cost of assimilating N— N_2 is nearly equivalent to that of N— NO_3^- (Großkopf and LaRoche, 2012). They are also consistent with an alternate cell flux modelling approach, which showed that the effect of the direct cost of N_2 fixation on growth efficiency was much smaller than the cost of protecting nitrogenase from O_2 inhibition in oxic conditions, which accounted for $>60\%$ of C substrate consumption at $192 \mu M O_2$ (Inomura et al., 2017). Our finding that the impact of N_2 fixation on overall growth yield is minimal ($<10\%$) at low ($<5 \mu M O_2$) can help explain why organic particles, where C is available and in which low O_2 microenvironments can form, act as sites for heterotrophic N_2 fixation in temperate estuaries (Pedersen et al., 2018) and, by extension, observed increases in heterotrophic diazotrophy following pulses of spring production in such systems (Bentzon-Tilia et al., 2015b).

4.3. Stoichiometry and energy yields of environmental C source drives N_2 fixation in the presence of exogenous fixed N

While N_2 fixation is commonly touted as an “energetically expensive” process, observations suggest that N_2 fixation is not always suppressed in the presence of “cheaper” N sources. Indeed, active diazotrophy has been detected across a range of pelagic and benthic riverine, estuarine, and marine environments in the presence of as much as $30 \mu M NO_3^-$ (typical of the deep sea) or $200 \mu M NH_4^+$ (typical of reducing sediments) (see Knapp, 2012 for summary), and may even be stimulated by exogenous N in some algal symbioses (Mills et al., 2020). Both *Azotobacter* (Bühler et al., 1987) and the cyanobacterium *Trichodesmium* (Mulholland and Capone, 2000) will assimilate NH_4^+ and N_2 simultaneously provided sufficient external energy inputs. Previous modeling work (Inomura et al., 2018) indicates that optimization of metabolisms under given resource availability explains the ratio of different N sources.

Under eutrophic reducing conditions with a highly labile C source (Scenario 5 with glucose; Section 3.4), typical of organic-rich sediments, we observed absolute N_2 fixation rates of a similar order of magnitude as those observed for pelagic systems under N-limitation (Fig. 4G-H). This observation is consistent with observations. Though benthic depositional environments (e.g., wetlands, marshes, mangroves, seagrasses, tidal flats) typically bear high ammonium concentrations due to active remineralization, a recent global compilation of studies across the aquatic spectrum (Fulweiler et al., 2025) found that measured N_2 fixation rates in such environments (with medians ranging from $5 \mu mol N m^{-2} h^{-2}$ for seagrasses to $45 \mu mol N m^{-2} h^{-2}$ for tidal flats) were on par with those measured in environments classically thought conducive to N_2 fixation (e.g., lake waters with a median rate of $17 \mu mol N m^{-2} h^{-2}$).

Our model provides a simple biological explanation for observations of N_2 fixation in the presence of fixed N (e.g., Bentzon-Tilia et al., 2015a; Fulweiler et al., 2025; Selden et al., 2019). N_2 fixation is triggered as the stoichiometric ratio of organic carbon available for heterotrophic metabolism and the reactive N available in the form of ammonium or nitrate (resource C:N) increases (Fig. 5). For example, our model indicates that N_2 fixation would be triggered in lake or estuarine sediments with an ammonium concentration of $100 \mu M$ in the porewaters, provided that the dissolved organic carbon (DOC) concentration was at least $400 \mu M$; it would be maximized if the DOC concentration was greater than or equal to 1.6 mM . Indeed, lake and estuarine sediments typically have DOC concentrations between $2 - 20 \text{ mM}$ (Wang et al., 2013; Ziegelgruber et al., 2013). These results show that organic-rich environments are likely to trigger substantial N_2 fixation regardless of the ammonium because the excess energy available in these environments does not limit nitrogenase synthesis/activity (Wang et al., 2021). Moreover, the relative importance of N_2 to growth need not be high for significant absolute N_2 fixation rates: In Scenario 5, we observed a high rate even though the relative contribution of N_2 to biomass N was $<4\%$

because high biomass was achieved given the labile C source (Fig. 3E-F).

4.4. Conclusions and future directions

Here we describe a novel model to quantify heterotrophic N_2 fixation that considers both mass and energetic requirements using ecological stoichiometry and microbial bioenergetic approaches, respectively. The inclusion of multiple terminal electron acceptors and N sources provides a framework for exploring environmental conditions that facilitate N_2 fixation. We incorporate both direct and indirect costs of nitrogen fixation under variable O_2 availability, which is important when considering tradeoffs between energetically favorable oxygenic respiration and costs to protect nitrogenase against oxygen inhibition.

Our model results demonstrate instances of N_2 fixation under both low environmental inorganic N concentrations, as expected, and under high environmental inorganic N concentrations historically thought to preclude N_2 fixation. Under relatively low concentrations of NO_3^- and NH_4^+ (Scenarios 2 and 4), N_2 fixation contributed ~30–75 % of N to biomass-N, depending on oxygen concentration and carbon energy yields/availability (Fig. 3E, F). Under replete fixed N scenarios (2, 3, 5), N_2 fixation contributed minimally (<4 %) to biomass N, depending on C substrate energy yields and availability (Fig. 3E, F; Fig. 5). Though the relative contribution was minimal (Fig. 3E-F), this N_2 fixation enabled high growth rates (Fig. 3C-D) and, consequently, absolute N_2 fixation rates similar to those observed under N-limitation under anoxic and eutrophic conditions when given a highly labile substrate (glucose) at a high concentration relative to the availability of exogenous N (Fig. 4G-H; see discussion in Section 3.4).

Based on these results, we proffer that observations of N_2 fixation in the presence of fixed N (e.g., Bentzon-Tilia et al., 2015a; Fulweiler et al., 2025; Selden et al., 2019) can be explained as follows: (a) Within an aerobic but low O_2 “Goldilock’s zone”, diazotrophs can gain a growth advantage by supplementing competitive fixed N ($NO_3^- + NH_4^+$) uptake with N_2 fixation, and (b) at nil to low-moderate O_2 concentrations, N_2 fixation is triggered as the stoichiometric availability of organic carbon relative to fixed N in the environment increases, provided a high energy-yield carbon substrate. If (b) occurs within (a), then a less rich carbon compound may be sufficient to drive diazotrophic. While we performed simulations using two carbon sources, this is simplistic relative to the diversity of carbon sources available in a natural environment. Future applications of this model which incorporate additional carbon sources or carbon mixtures would help us understand how carbon quality may impact the bioenergetics of heterotrophic N_2 fixation.

While the model results presented here explored N_2 fixation in scenarios representing variable resource availability, parameters related to the physiological traits of heterotrophic diazotrophs remained fixed throughout these trials (see Section 3.6). Nonetheless, heterotrophic diazotrophs are a physiologically diverse group. In depth exploration of N_2 fixation across heterotrophic diazotrophs that vary in their substrate uptake rates, half saturation constants, and the range of biomass N:C ratios (Q_{min} and Q_{max}) is a warranted next step for exploring the physiological controls of N_2 fixation in diazotrophic heterotrophs.

Funding

This work was supported by National Science Foundation award #2015825. CRS thanks the Rutgers University Presidential Postdoctoral Fellowship Program for supporting her time during this project. HMH acknowledges support from NSF EPSCoR Track-2 FEC Award #2019596. Additional support was provided by NASA MUREP grant #80NSSC22K1242 (ECR and JP).

Data statement

All data and code are publicly available for re-use. Full model MATLAB code can be downloaded from Zenodo (DOI: 10.5281/

zenodo.14926970). All extracted parameters and associated references are found in Supplement C.

CRediT authorship contribution statement

Corday R. Selden: Writing – review & editing, Writing – original draft, Visualization, Methodology, Investigation, Formal analysis, Conceptualization. **Rebecca A. Everett:** Writing – review & editing, Writing – original draft, Visualization, Validation, Methodology, Investigation, Formal analysis, Conceptualization. **Halvor M. Halvorson:** Writing – review & editing, Writing – original draft, Methodology, Investigation, Data curation, Conceptualization. **Megan E. Berberich:** Writing – review & editing, Writing – original draft, Project administration, Methodology, Investigation, Formal analysis, Conceptualization. **Luca Schenone:** Writing – review & editing, Writing – original draft, Visualization, Methodology, Investigation, Formal analysis, Conceptualization. **Angela Peace:** Writing – review & editing, Writing – original draft, Visualization, Validation, Methodology, Investigation, Formal analysis. **Renn Schipper:** Writing – review & editing, Writing – original draft, Data curation, Conceptualization. **Edwin Cruz-Rivera:** Writing – review & editing, Writing – original draft, Visualization, Data curation, Conceptualization. **James Powell:** Writing – review & editing, Data curation. **Keisuke Inomura:** Writing – review & editing, Methodology. **Robinson W. Fulweiler:** Writing – review & editing, Supervision, Funding acquisition, Conceptualization. **Amy M. Marcarelli:** Writing – review & editing, Supervision, Funding acquisition, Conceptualization. **J. Thad Scott:** Writing – review & editing, Writing – original draft, Supervision, Methodology, Investigation, Funding acquisition, Formal analysis, Conceptualization.

Declaration of competing interest

The authors declare the following financial interests/personal relationships which may be considered as potential competing interests:

Amy Marcarelli, Wally Fulweiler, Thad Scott reports financial support was provided by National Science Foundation. If there are other authors, they declare that they have no known competing financial interests or personal relationships that could have appeared to influence the work reported in this paper.

Acknowledgements

We gratefully acknowledge the broader members of the Aquatic N_2 fixation Research Collaboration Network for their encouragement, guidance, and feedback. In particular, we thank Bob Sterner (Univ. of Minn. Duluth) for encouraging us to consider how to incorporate microbial bioenergetics into an ecological stoichiometry framework, and Jim Cotner (Univ. of Minn. Twin Cities) and Julian Damashek (Hamilton College) for their careful review of this manuscript prior to publication. We are further grateful to Sergei Katsev (Univ. of Minn. Duluth) for offering consult regarding the structure of our Gibbs energy dissipation model.

Supplementary materials

Supplementary material associated with this article can be found, in the online version, at [doi:10.1016/j.ecolmodel.2025.111454](https://doi.org/10.1016/j.ecolmodel.2025.111454).

Data availability

The data used in this article was sourced from prior literature and is available in Supplement C.

References

- Andersen, K., Shanmugam, K., 1977. Energetics of biological nitrogen fixation: determination of the ratio of formation of H₂ to NH₄⁺ catalysed by nitrogenase of *Klebsiella pneumoniae* in vivo. *Microbiology* 103, 107–122.
- Bentzon-Tilia, M., Severin, I., Hansen, L.H., Riemann, L., 2015a. Genomics and ecophysiology of heterotrophic nitrogen-fixing bacteria isolated from estuarine surface water. *MBio* 6, 10–1128.
- Bentzon-Tilia, M., Traving, S.J., Mantikci, M., Knudsen-Leerbeck, H., Hansen, J.L., Markager, S., Riemann, L., 2015b. Significant N₂ fixation by heterotrophs, photoheterotrophs and heterocystous cyanobacteria in two temperate estuaries. *ISME J.* 9, 273–285.
- Bühler, T., Sann, R., Monter, U., Dingler, C., Kuhla, J., Oelze, J., 1987. Control of dinitrogen fixation in ammonium-assimilating cultures of *Azotobacter vinelandii*. *Arch. Microbiol.* 148, 247–251.
- Burdige, D.J., Zheng, S., 1998. The biogeochemical cycling of dissolved organic nitrogen in estuarine sediments. *Limnol. Ocean.* 43, 1796–1813.
- Calabrese, S., Chakrawal, A., Manzoni, S., Van Cappellen, P., 2021. Energetic scaling in microbial growth. *Proc. Natl. Acad. Sci.* 118, e2107668118.
- Castillo, T., García, A., Padilla-Córdova, C., Díaz-Barrera, A., Peña, C., 2020. Respiration in *Azotobacter vinelandii* and its relationship with the synthesis of biopolymers. *Elect. J. Biotech.* 48, 36–45. <https://doi.org/10.1016/j.ejbt.2020.08.001>.
- Chakraborty, S., Andersen, K.H., Merico, A., Riemann, L., 2025. Particle-associated N₂ fixation by heterotrophic bacteria in the global ocean. *Sci. Adv.* 11, eadq4693.
- Chakraborty, S., Andersen, K.H., Visser, A.W., Inomura, K., Follows, M.J., Riemann, L., 2021. Quantifying nitrogen fixation by heterotrophic bacteria in sinking marine particles. *Nat. Commun.* 12, 4085.
- Del Giorgio, P., Davis, J., 2003. Patterns in dissolved organic matter lability and consumption across aquatic ecosystems. *Aquatic Ecosystems*. Elsevier, pp. 399–424.
- Del Giorgio, P.A., Cole, J.J., 1998. Bacterial growth efficiency in natural aquatic systems. *Ann. Rev. Ecol. Syst.* 29, 503–541.
- Dodds, W.K., 2006. Nutrients and the “dead zone”: the link between nutrient ratios and dissolved oxygen in the northern Gulf of Mexico. *Front. Ecol. Environ.* 4, 211–217.
- Droop, M.R., 1973. Some thoughts on nutrient limitation in algae. *J. Phycol.* 9, 264–272. <https://doi.org/10.1111/j.1529-8817.1973.tb04092.x>.
- Durand, P., Breuer, L., Johns, P.J., Billen, G., Butturini, A., Pinay, G., van Grinsven, H., Garnier, J., Rivett, M., Reay, D.S., 2011. Nitrogen processes in aquatic ecosystems. Falkowski, P., 1983. Enzymology of nitrogen assimilation, in: Nitrogen in the marine environment.
- Fulweiler, R., Brown, S., Nixon, S., Jenkins, B., 2013. Evidence and a conceptual model for the co-occurrence of nitrogen fixation and denitrification in heterotrophic marine sediments. *Mar. Ecol. Prog. Series* 482, 57–68.
- Fulweiler, R.W., 2023. More foxes than hedgehogs: the case for nitrogen fixation in coastal marine sediments. *Glob. Biogeochem. Cycles* 37, e2023GB007777. <https://doi.org/10.1029/2023GB007777>.
- Fulweiler, R.W., Berberich, M.E., Rinehart, S.A., Taylor, J.M., Kelly, M.C., Ray, N.E., Oczkowski, A., Balint, S.J., Geisser, A.H., Mahoney, C.R., 2025. A global dataset of nitrogen fixation rates across inland and coastal waters. *Limnol. Ocean. Lett.*
- Godwin, C.M., Cotner, J.B., 2015. Stoichiometric flexibility in diverse aquatic heterotrophic bacteria is coupled to differences in cellular phosphorus quotas. *Front. Microbiol.* 6. <https://doi.org/10.3389/fmicb.2015.00159>.
- González-Cabaleiro, R., Ofițeru, I.D., Lema, J.M., Rodríguez, J., 2015. Microbial catabolic activities are naturally selected by metabolic energy harvest rate. *ISME J.* 9, 2630–2641. <https://doi.org/10.1038/ismej.2015.69>.
- Großkopf, T., LaRoche, J., 2012. Direct and indirect costs of dinitrogen fixation in *Crocospaera watsonii* WH8501 and possible implications for the nitrogen cycle. *Front. Microbiol.* 3, 236.
- Gutschick, V.P., 2005. Energetics of microbial fixation of dinitrogen. *Microbes and Engineering Aspects*. Springer, pp. 109–167.
- Heijnen, J., van Loosdrecht, M.C., Tijhuis, L., 1992. A black box mathematical model to calculate auto- and heterotrophic biomass yields based on Gibbs energy dissipation. *Biotech. Bioeng.* 40, 1139–1154.
- Heijnen, J.J., Van Dijken, J.P., 1992. In search of a thermodynamic description of biomass yields for the chemotrophic growth of microorganisms. *Biotech. Bioeng.* 39, 833–858. <https://doi.org/10.1002/bit.260390806>.
- Hessen, D.O., Elser, J.J., Sterner, R.W., Urabe, J., 2013. Ecological stoichiometry: an elementary approach using basic principles. *Limnol. Ocean.* 58, 2219–2236.
- Inomura, K., Bragg, J., Follows, M.J., 2017. A quantitative analysis of the direct and indirect costs of nitrogen fixation: a model based on *Azotobacter vinelandii*. *ISME J.* 11, 166–175.
- Inomura, K., Bragg, J., Riemann, L., Follows, M.J., 2018. A quantitative model of nitrogen fixation in the presence of ammonium. *PLoS One* 13, e0208282.
- Inomura, K., Deutsch, C., Masuda, T., Prášil, O., Follows, M.J., 2020. Quantitative models of nitrogen-fixing organisms. *Comput. Struct. Biotech. J.* 18, 3905–3924.
- Knapp, A.N., 2012. The sensitivity of marine N₂ fixation to dissolved inorganic nitrogen. *Front. Microbiol.* 3, 374.
- Koirala, A., Brözel, V.S., 2021. Phylogeny of nitrogenase structural and assembly components reveals new insights into the origin and distribution of nitrogen fixation across bacteria and archaea. *Microorganisms* 9, 1662.
- Kuhla, J., Oelze, J., 1988. Dependency of growth yield, maintenance and K_s-values on the dissolved oxygen concentration in continuous cultures of *Azotobacter vinelandii*. *Arch. Microbiol.* 149, 509–514.
- Marcarelli, A.M., Fulweiler, R.W., Scott, J.T., 2022. Nitrogen fixation: a poorly understood process along the freshwater-marine continuum. *Limnol. Oceanogr. Lett.* 7, 1–10. <https://doi.org/10.1002/lo.10220>.
- Marino, S., Hogue, I.B., Ray, C.J., Kirschner, D.E., 2008. A methodology for performing global uncertainty and sensitivity analysis in systems biology. *J. Theor. Biol.* 254, 178–196.
- Michaelis, L., Menten, M.L., 1913. Die kinetik der invertinwirkung. *Biochem. Z.* 49, 352.
- Mills, M.M., Turk-Kubo, K.A., van Dijken, G.L., Henke, B.A., Harding, K., Wilson, S.T., Arrigo, K.R., Zehr, J.P., 2020. Unusual marine cyanobacteria/haptophyte symbiosis relies on N₂ fixation even in N-rich environments. *ISME J.* 14, 2395–2406.
- Mulholland, M.R., Capone, D.G., 2000. The nitrogen physiology of the marine N₂-fixing cyanobacteria *Trichodesmium* spp. *Trend. Plant Sci.* 5, 148–153.
- Münster, U., 1993. Concentrations and fluxes of organic carbon substrates in the aquatic environment. *Antonie van Leeuwenhoek* 63, 243–274.
- Pate, J.S., Layzell, D.B., Mifflin, B., Lea, P., 1990. Energetics and biological costs of nitrogen assimilation. *Biochem. Plants* 16, 1–42.
- Pawlowski, R., Baldwin, S.A., Muttray, A., Schmidtova, J., Laval, B., Lamont, G., 2007. Physical, chemical, and microbial regimes in an anoxic fjord (Nitinat Lake). *Limnol. Ocean.* 52, 1002–1017.
- Pedersen, J.N., Bombar, D., Paerl, R.W., Riemann, L., 2018. Diazotrophs and N₂-fixation associated with particles in coastal estuarine waters. *Front. Microbiol.* 9, 2759.
- Penocchio, E., Rao, R., Esposito, M., 2019. Thermodynamic efficiency in dissipative chemistry. *Nat. Commun.* 10, 3865.
- Pierella Karlusich, J.J., Pelletier, E., Lombard, F., Carsique, M., Dvorak, E., Colin, S., Picheral, M., Cornejo-Castillo, F.M., Acinas, S.G., Pepperkok, R., 2021. Global distribution patterns of marine nitrogen-fixers by imaging and molecular methods. *Nat. Commun.* 12, 4160.
- Poole, R.K., Hill, S., 1997. Respiratory Protection of Nitrogenase Activity in *Azotobacter vinelandii*—Roles of the Terminal Oxidases. *Biosci. Rep.* 17, 303–317. <https://doi.org/10.1023/A:1027336712748>.
- Post, E., Goleccki, J., Oelze, J., 1982. Morphological and ultrastructural variations in *Azotobacter vinelandii* growing in oxygen-controlled continuous culture. *Arch. Microbiol.* 133, 75–82.
- Post, E., Kleiner, D., Oelze, J., 1983. Whole cell respiration and nitrogenase activities in *Azotobacter vinelandii* growing in oxygen controlled continuous culture. *Arch. Microbiol.* 134, 68–72.
- Redfield, A.C., 1958. The biological control of chemical factors in the environment. *Am. Sci.* 46, 230A–2221.
- Sabra, W., Zeng, A.P., Lünsdorf, H., Deckwer, W.D., 2000. Effect of oxygen on formation and structure of *Azotobacter vinelandii* alginate and its role in protecting nitrogenase. *Appl. Environ. Microbiol.* 66, 4037–4044. <https://doi.org/10.1128/AEM.66.9.4037-4044.2000>.
- Scott, J.T., Stanley, J.K., Doyle, R.D., Forbes, M.G., Brooks, B.W., 2009. River–reservoir transition zones are nitrogen fixation hot spots regardless of ecosystem trophic state. *Hydrobiologia* 625, 61–68.
- Selden, C., Mulholland, M., Bernhardt, P., Widner, B., Macías-Tapia, A., Ji, Q., Jayakumar, A., 2019. Dinitrogen fixation across physico-chemical gradients of the Eastern Tropical North Pacific oxygen deficient zone. *Glob. Biogeochem. Cycl.* 33, 1187–1202.
- Selden, C., Mulholland, M., Crider, K., Clayton, S., Macías-Tapia, A., Bernhardt, P., McGillicuddy Jr, D., Zhang, W., Chappell, P., 2024. Nitrogen fixation at the Mid-Atlantic Bight shelfbreak and transport of newly fixed nitrogen to the Slope Sea. *J. Geophys. Res.* 129, e2023JC020651.
- Selden, C.R., Mulholland, M.R., Widner, B., Bernhardt, P., Jayakumar, A., 2021. Toward resolving disparate accounts of the extent and magnitude of nitrogen fixation in the Eastern Tropical South Pacific oxygen deficient zone. *Limnol. Ocean.* 66, 1950–1960.
- Smeaton, C.M., Van Cappellen, P., 2018. Gibbs Energy Dynamic Yield Method (GEDYM): Predicting microbial growth yields under energy-limiting conditions. *Geochimica et Cosmochimica Acta* 241, 1–16.
- Stam, H., Stouthamer, A.H., van Verseveld, H.W., 1987. Hydrogen metabolism and energy costs of nitrogen fixation. *FEMS Microbiol. Rev.* 3, 73–92.
- Sterner, R., Elser, J., 2003. Ecological stoichiometry: The biology of Elements from Biomolecules to the Biosphere. Princeton University Press.
- Testa, J.M., Kemp, W.M., Boynton, W.R., 2018. Season-specific trends and linkages of nitrogen and oxygen cycles in Chesapeake Bay. *Limnol. Ocean.* 63, 2045–2064.
- Turk-Kubo, K.A., Gradoville, M.R., Cheung, S., Cornejo-Castillo, F.M., Harding, K.J., Morando, M., Mills, M., Zehr, J.P., 2022. Non-cyanobacterial diazotrophs: Global diversity, distribution, ecophysiology, and activity in marine waters. *FEMS Microbiol. Rev.*
- Vitousek, P.M., Menge, D.N., Reed, S.C., Cleveland, C.C., 2013. Biological nitrogen fixation: rates, patterns and ecological controls in terrestrial ecosystems. *Philos. Trans. R. Soc. B Biol. Sci.* 368, 20130119.
- Wang, J., Wu, Y., Li, J., He, Q., Zhu, H., Bing, H., 2021. Energetic supply regulates heterotrophic nitrogen fixation along a glacial chronosequence. *Soil Biol. Biochem.* 154, 108150. <https://doi.org/10.1016/j.soilbio.2021.108150>.
- Wang, Y., Zhang, D., Shen, Z., Feng, C., Chen, J., 2013. Revealing sources and distribution changes of dissolved organic matter (DOM) in pore water of sediment from the Yangtze Estuary. *PLoS One* 8, e76633. <https://doi.org/10.1371/journal.pone.0076633>.
- Ziegelgruber, K.L., Zeng, T., Arnold, W.A., Chin, Y.P., 2013. Sources and composition of sediment pore-water dissolved organic matter in prairie pothole lakes. *Limnol. Ocean.* 58, 1136–1146. <https://doi.org/10.4319/lo.2013.58.3.1136>.